

Line-of-Sight-Constrained Multi-Robot Mapless Navigation via Polygonal Visible Region

Ruofei Bai, Shenghai Yuan, Xinhang Xu, Xingyu Ji, Xiaowei Li, Hongliang Guo, Wei-Yun Yau, Lihua Xie

Abstract—Multi-robot systems rely on underlying connectivity to ensure reliable communication and timely coordination. This paper studies the line-of-sight (LoS) connectivity maintenance problem in multi-robot navigation with unknown obstacles. Prior works typically assume known environment maps to formulate LoS constraints between robots, which hinders their practical deployment. To overcome this limitation, we propose an inherently distributed approach where each robot only constructs an egocentric visible region based on its real-time LiDAR scans, instead of endeavoring to build a global map online. The individual visible regions are shared through distributed communication to establish inter-robot LoS constraints, which are then incorporated into a multi-robot navigation framework to ensure LoS-connectivity. Moreover, we enhance the robustness of connectivity maintenance by proposing a more accurate LoS-distance metric, which further enables network topology optimization by eliminating redundant and effort-demanding connections for improved navigation efficiency. The proposed framework is evaluated through extensive multi-robot navigation and exploration tasks in both simulation and real-world experiments. Results show that it reliably maintains LoS-connectivity between robots in challenging environments cluttered with obstacles, even under large visible ranges and fragile minimal topologies, where existing methods consistently fail. Ablation studies also reveal that topology optimization boosts navigation efficiency by around 20%, demonstrating the framework’s potential for efficient navigation under connectivity constraints.

I. INTRODUCTION

Multi-robot navigation holds numerous applications in search and rescue [1], collaborative inspection [2], and autonomous exploration [3]. While individual robots have limited onboard communication and sensing capabilities, multi-robot systems can overcome such limitations and operate in wider areas. To ensure reliable inter-robot communication and timely coordination, it is essential to maintain a connected network between robots [4]. However, existing methods usually omit the presence of obstacles that degrade signals and prevent mutual observation between robots [5], thereby compromising information sharing and mutual observation [6]. To this end, this paper considers a situation where each robot in a team must be within at least one of its neighbors’ *line-of-sight* (LoS) and communication range to be connected, while avoiding collisions, as shown in Fig. 1. The problem is challenging as robots need to maintain LoS-connectivity in the presence of obstacles while performing external navigation tasks [4].

Prior studies on related problems typically assume known environmental models [4], [8], [9], [10], where obstacles are either represented by a predefined set of obstacle points [9], [4], [11], or a shared occupancy map between robots [5].

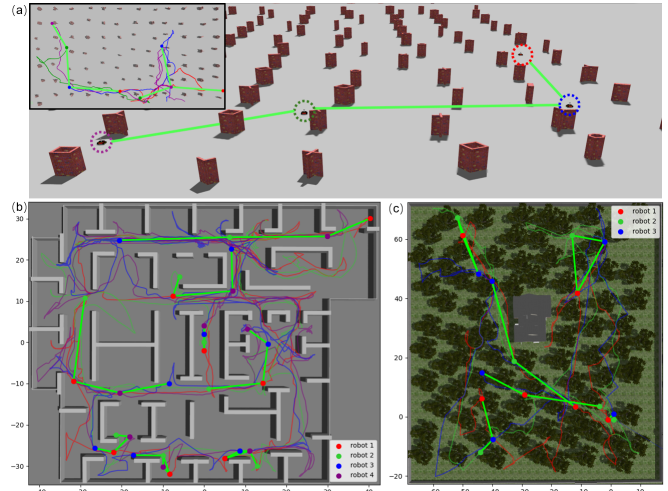


Fig. 1. (a) Four robots navigate in a simulation environment cluttered with small irregular obstacles while always maintaining LoS-connectivity ($100m \times 50m$). (b) The trajectories of four robots and snapshots of their connectivity graphs when exploring an initially unknown garage environment [3] ($87m \times 69m$). (c) Three robots exploring an outdoor forest environment adapted from [7] ($86m \times 95m$).

However, reliance on prior maps prevents above methods from real-world applications, where the environment can be unknown with unpredictable and irregular obstacles that obstruct LoS connectivity between robots. Moreover, it remains a non-trivial task to collaboratively build a map among robots to verify their LoS-connectivity during online operation.

To eliminate the requirements on prior maps, we propose a novel idea that, instead of endeavoring to construct a shared global map, each robot only needs to explicitly construct an egocentric *visible region* based on its real-time LiDAR scans. The visible region describes the space that is currently visible from a robot, which is shared between neighboring robots to formulate their inter-robot LoS constraints. The LoS constraints are then integrated into a graph Laplacian-based controller [9] for connectivity maintenance. Although preliminary work is proposed in [12], it suffers from brittle connectivity due to the inaccurate LoS-distance metric and inefficient navigation caused by redundant connections. Motivated by these limitations, we make substantial modifications to achieve more robust LoS-connectivity maintenance and flexible navigation behaviors. In particular, we reformulate a polygonal approximation of visible regions to support accurate LoS-distance evaluation, and propose an online topology optimization approach that facilitates robots’ navigation efficiency. Consequently, our method can reliably maintain global connectivity of robots

even with fragile topologies and large visible ranges, while previous methods fail under such conditions. Our contributions are summarized as follows:

- 1) We propose a polygonal approximation of a robot's visible region constructed from real-time LiDAR scans, which supports an efficient and reliable metric for LoS-distance evaluation between robots;
- 2) We prove that the proposed metric lower-bounds the actual LoS distance, serving as a safe and conservative approximation regardless of the coverage range of visible regions.
- 3) We propose a topology optimization approach in graph Laplacian-based controllers, where the network topology is flexibly adapted to minimize the efforts for connectivity maintenance between robots considering external navigation tasks.

The robustness and efficiency of the proposed method is extensively evaluated with multi-robot navigation and exploration tasks in unknown cluttered environments, where robots can successfully navigate to their targets while robustly maintaining LoS-connectivity. We also validate the applicability of the proposed framework in real-world experiments.

II. RELATED WORKS

A. Line-of-Sight-Constrained Multi-Robot Navigation

Existing work considering LoS-connectivity maintenance can be categorized into continuous and discrete types [4], where LoS constraints are usually formulated based on known global maps, such as obstacle points [9], [13], occupancy maps [14], [8], etc. Giordano *et al.* proposed a potential function-based method that guarantees continuous connectivity by preserving the positivity of the Fiedler eigenvalue [9], [4]. The LoS constraints are captured by the distance from the closest obstacle point to the LoS segment joining two robots. Chen *et al.* consider the LoS constraints in multi-UAV deployment by restricting two robots to be within a common separating hyperplane of obstacles [11]. In contrast, discrete connectivity only requires robots to be connected at certain time steps [15]. Typically, a *target topology* is first determined to ensure connectivity and then optimized to consider additional objectives, such as distance or information gain [5], [14], [16], [8]. Xia *et al.* formulate the LoS constraints based on robots' visible regions described by star convex polytopes [8]. However, as *local optimization* modifies robots' positions, the corresponding changes in their visible regions may lead to potential loss of LoS after optimization.

As a preliminary attempt to alleviate the reliance on prior maps, Bai *et al.* mitigate the limitation of [8] by applying the concept of visible region (constructed from onboard LiDAR scans) to continuous connectivity maintenance [12]. However, it suffers from brittle connectivity due to the inaccurate LoS-distance metric and inefficient navigation. The above limitations are addressed in this work through a more reliable metric that supports robust LoS maintenance, which further enables flexible topology optimization for efficient robot navigation.

B. Topology Optimization in Connectivity Maintenance

Ensuring team connectivity often imposes constraints on robot navigation. To alleviate this, previous studies have proposed maintaining only the necessary connections among robots rather than preserving all of them [8], [5]. Shi *et al.* studied the topology optimization in a communication-constrained multi-robot exploration problem [5], where robots' future positions are first selected to maximize coverage, and then refined with minimum deviations to form a connected minimum spanning tree (MST). Xie *et al.* studied the problem of deploying the minimum number of robots to relay messages between a base station and several client points [8]. A Steiner Tree is optimized to determine the positions of relay robots that connect the base station to the target clients. Similar to our work, Yang *et al.* studied the minimally LoS-connectivity constrained multi-robot coordination problem, where only a selected minimum spanning tree is maintained with control barrier functions [13], [17]. Inspired by this work, we introduce a convenient topology optimization method within a graph Laplacian-based connectivity controller, which prunes unnecessary connections that require substantial effort to maintain under external navigation tasks, thereby improving navigation efficiency.

III. PRELIMINARIES

A. Graph Laplacian and Generalized Graph Connectivity

Given a graph $\mathcal{G} = \langle \mathcal{V}, \mathcal{E} \rangle$ with N vertices, the graph Laplacian matrix of \mathcal{G} is defined as $\mathbf{L} = \mathbf{D} - \mathbf{A}$, where $\mathbf{A} \in \mathbb{R}^{N \times N}$ is the adjacency matrix with an element $A_{ij} = 0$ if $(i, j) \notin \mathcal{E}$, and $A_{ij} > 0$ otherwise; $\mathbf{D} \in \mathbb{R}^{N \times N}$ is a diagonal degree matrix where $D_{ii} = \sum_{j=1}^N A_{ij}$ and $D_{ij} = 0$ when $i \neq j$. The second-smallest eigenvalue λ_2 of \mathbf{L} , usually referred to as the Fiedler eigenvalue [19], can be used to check the connectivity of \mathcal{G} . It holds the property that $\lambda_2 > 0$ if the graph \mathcal{G} is connected; otherwise, $\lambda_2 = 0$ if \mathcal{G} is disconnected.

By encoding the satisfaction of inter-robot connectivity constraints into the edge weight A_{ij} , the Fiedler eigenvalue λ_2 of the *weighted* graph Laplacian matrix of robots' underlying connectivity graph can reflect the *generalized* graph connectivity [9]. As in [9], [10], after defining a potential function $V^\lambda(\lambda_2) = \frac{1}{\lambda_2 - \lambda_2^{\min}}$ to enforce the Fiedler eigenvalue λ_2 being larger than a preferred lower bound $\lambda_2^{\min} > 0$, the gradient direction for a robot $i \in \mathcal{R}$ to maintain the connectivity of \mathcal{G} can be derived as [20]

$$\mathbf{u}_i^c = -\frac{\partial V^\lambda(\lambda_2)}{\partial \lambda_2} \cdot \frac{\partial \lambda_2}{\partial \mathbf{q}_i} = -\frac{\partial V^\lambda(\lambda_2)}{\partial \lambda_2} \cdot \sum_{j \in \mathcal{N}_i} \frac{\partial A_{ij}}{\partial \mathbf{q}_i} (v_{2_i} - v_{2_j})^2, \quad (1)$$

where v_{2_i} and v_{2_j} are the i -th and j -th elements of the normalized eigenvector \mathbf{v}_2 corresponding to λ_2 , respectively. Following the above concepts, this work ensures LoS-connectivity between robots by encoding connectivity constraints into the weighted graph Laplacian matrix of robots' underlying graphs.

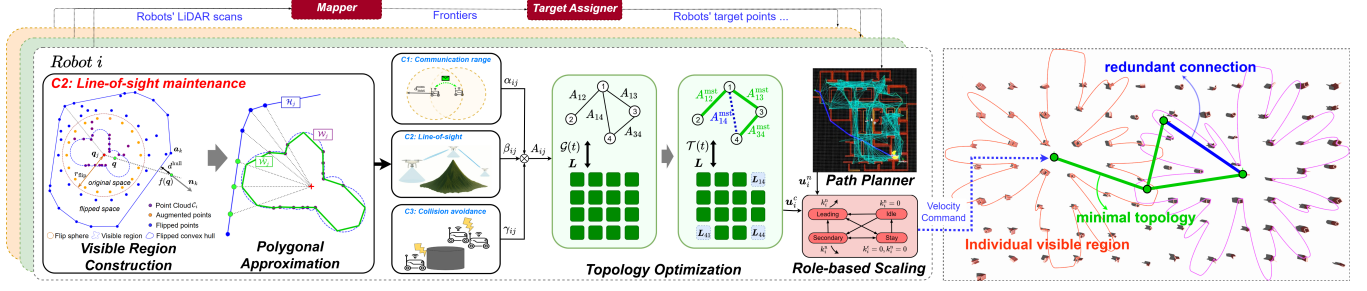


Fig. 2. Framework of LoS-connectivity constrained multi-robot navigation method. Each robot independently constructs its visible region with the polygonal approximation, based on real-time LiDAR scans. After sharing with immediate neighbors, three types of connectivity constraints are formulated as the weight of the robots' connectivity graph, which is then proceeded with topology optimization. Next, the masked graph Laplacian matrix is used to derive the connectivity velocity \mathbf{u}_i^c , which is then fused with external navigational velocity \mathbf{u}_i^n through the role-based scaling module, following the design in [12]. Finally, each robot is driven independently by the fused velocity command to maintain LoS-connectivity between robots while navigating to its own target. The navigational velocity is obtained from a mapless path planner proposed in [18]. The framework can also be extended for multi-robot exploration by integrating a multi-robot mapper for frontier extraction and a navigation-target assigner, as exemplified in Fig. 1(b)(c).

B. Visible Region Construction from Point Cloud

This work eliminates the requirements of prior known maps by constructing a real-time egocentric visible region for individual robot based on its onboard LiDAR scans. The process is adapted from visibility analysis techniques in computer graphics [21]. As shown in Fig. 2, given a point cloud $\mathcal{C}_j \subseteq \mathbb{R}^3$ of a robot j , its visible region can be constructed with the following four steps [21]: 1) Augmentation. Add augmented points to fill the gaps in the point cloud \mathcal{C}_j ; 2) Spherical flipping. Flip each point $\mathbf{q} \in \mathcal{C}_j$ to a point $\mathbf{q}' = f(\mathbf{q})$ located outside a sphere with a predefined radius r_{flip} , where $r_{\text{flip}} > \|\mathbf{q}\|$ and $f(\cdot)$ is the spherical flipping function defined as

$$f: \mathbf{q} \rightarrow 2r_{\text{flip}} \cdot \frac{\mathbf{q}}{\|\mathbf{q}\|} - \mathbf{q}. \quad (2)$$

The flipped point cloud is denoted as \mathcal{C}'_j ; 3) Convex hull construction. Generate a convex hull of \mathcal{C}'_j , denoted as \mathcal{H}_j ; 4) Inversion. Inverse the boundary of \mathcal{H}_j by performing spherical flipping again. The inversed boundary encloses the visible region of robot j , denoted as \mathcal{W}_j . By construction, a larger r_{flip} determines a larger visible region [21], [8].

Definition 1 (Visible Region): Given the point cloud \mathcal{C}_j of a robot j , and its corresponding convex hull \mathcal{H}_j with K faces, the visible region is defined as

$$\mathcal{W}_j = \{\mathbf{q} \mid \max_{k \in [1, \dots, K]} \{\mathbf{n}_k^\top (f(\mathbf{q}) - \mathbf{a}_k)\} > 0\} \subseteq \mathbb{R}^3,$$

where \mathbf{n}_k is the outward normal vector of the k -th face of \mathcal{H}_j , and $\mathbf{a}_k \in \mathbb{R}^3$ is a vertex point on the k -th face.

Proposition 1 (Visibility Determination [21]): A point $\mathbf{q} \in \mathbb{R}^3$ is within the LoS of a robot j if $\mathbf{q} \in \mathcal{W}_j$; or equivalently, a determination metric $d^{\text{hull}} > 0$, where $d^{\text{hull}} = \max\{d_k = \mathbf{n}_k^\top (f(\mathbf{q}) - \mathbf{a}_k) \mid k = 1, \dots, K\}$ for \mathcal{H}_j with K faces.

A differentiable approximation of the determination metric d^{hull} can be defined with the log-sum-exp relaxation as

$$d^{\text{hull}} \approx \frac{1}{\alpha} \log(e^{\alpha d_1} + \dots + e^{\alpha d_K}), \quad (3)$$

where $\alpha > 0$ is a coefficient that controls the degree of approximation [22].

IV. PROBLEM FORMULATION

A. Robot Model

Assume there are a set of robots $\mathcal{R} = \{1, 2, \dots, R\}$ navigating in an initially unknown environment. The position of a robot $i \in \mathcal{R}$ at time t is denoted as $\mathbf{q}_i(t) \in \mathbb{R}^3$. Its kinematic model is given by

$$\mathbf{q}_i(t+1) = \mathbf{q}_i(t) + \mathbf{u}_i(t), \quad (4)$$

where $\mathbf{u}_i(t) = k_i^c \cdot \mathbf{u}_i^c(t) + k_i^n \cdot \mathbf{u}_i^n(t)$; $\mathbf{u}_i^c, \mathbf{u}_i^n \in \mathbb{R}^{2,3}$ are the velocity commands for connectivity and navigation, respectively; and $k_i^c, k_i^n \in \mathbb{R}_{\geq 0}$ are two scaling factors. Moreover, $\|\mathbf{u}_i(t)\|_2 \leq U_{\text{max}}$, where U_{max} is the upper limit of robots' velocities.

B. Connectivity Constraints

Let $\mathcal{G}(t) = \langle \mathcal{V}, \mathcal{E}(t), \omega \rangle$ be an undirected time-varying connectivity graph of robots, where $\mathcal{V} = \{1, \dots, R\}$ includes R vertices corresponding to robots in \mathcal{R} ; $\mathcal{E}(t) \subseteq \mathcal{V} \times \mathcal{V}$ is the edge set at time t ; and the weighting function $\omega: \mathcal{V} \times \mathcal{V} \rightarrow \mathbb{R}_{\geq 0}$ evaluates the strength of edge between two vertices in the graph. An edge (i, j) exists between two robots i and j if and only if the following constraints are satisfied, where $d_{ij} = \|\mathbf{q}_i - \mathbf{q}_j\|_2$.

- (C1) Communication range. The distance d_{ij} must be within a communication range $d_{\text{max}}^{\text{com}}$, i.e., $d_{ij} \leq d_{\text{max}}^{\text{com}}$.
- (C2) Line-of-Sight maintenance. The two robots must be within each other's line-of-sight, i.e., $\eta \mathbf{q}_i + (1 - \eta) \mathbf{q}_j \notin \mathcal{O}$, $\forall \eta \in [0, 1]$, where $\mathcal{O} \subseteq \mathbb{R}^3$ denotes the space occupied by obstacles.
- (C3) Collision avoidance. The inter-robot and robot-obstacle distances must be no less than a safe distance $d_{\text{min}}^{\text{coll}}$, i.e., $d_{ij} \geq d_{\text{min}}^{\text{coll}}$, $\min_{\mathbf{q} \in \mathcal{O}} \|\mathbf{q}_i - \mathbf{q}\|_2 \geq d_{\text{min}}^{\text{coll}}$.

We define $\omega(\cdot)$ as $\omega(i, j) = A_{ij} = \alpha_{ij} \cdot \beta_{ij} \cdot \gamma_{ij}$, where $\alpha(\cdot), \beta(\cdot), \gamma(\cdot)$ are three potential functions to quantify the satisfaction of constraints C1, C2, and C3 between robots, respectively. As the functions $\alpha(\cdot)$ and $\gamma(\cdot)$ only depend on robots' relative distances regardless of the environment, we define them following [12]. We instead focus on formulating $\beta(\cdot)$ in this paper. Initially, we assume $\mathcal{G}(0)$ is connected.

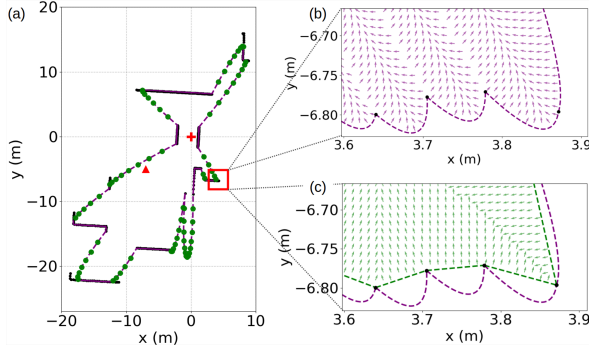


Fig. 3. (a): A robot (denoted by +) with its visible region and polygonal approximation, whose boundaries are highlighted by purple and green dotted lines in (b) and (c), respectively. The radial angle-based interpolation adapts to the boundary geometry by placing denser points (green dots in (a)) along boundaries of high curvature and sparser points along flatter boundaries. (b) and (c) also show the gradient field of d^{hull} (purple arrows) and d^{los} (green arrows) respectively, in a zoomed-in area. A probe point (denoted by \blacktriangle) in (a) has the exact $d^{\text{los}} = 1.08m$ and $\tilde{d}^{\text{los}} = 1.07m$, while $d^{\text{hull}} = 12.50m$ showing significant metric error. Moreover, the gradient of d^{hull} tends to trap a robot within a small radial sector.

C. Problem Statement

Given a sequence of target points $\mathcal{Z} = \{z^1, \dots, z^M\} \subseteq \mathbb{R}^3$ distributed in the free space of an unknown environment, and a group of robots $\mathcal{R} = \{1, \dots, R\}$ with kinematic models defined in Eq. (4). We assume $M \leq R$, and a target $z^m \in \mathcal{Z}$ is assigned to a robot $i^m \in \mathcal{R}$. $\forall t \geq 0$, the problem is to find a sequence of velocity commands $\mathbf{u}_i(t)$ for each robot $i \in \mathcal{R}$ so that: (1) there exists a time sequence $0 \leq t^1, \dots, t^M < \infty$ when a target z^m is visited by the assigned robot i^m at time t^m ; (2) the connectivity graph $\mathcal{G}(t)$ is always connected; (3) the time required to visit all targets is minimized.

The key challenge lies in reliably maintaining LoS connectivity between robots in unknown environments while minimizing the impact on their external navigation tasks, which is discussed in the following sections.

V. METHODOLOGY

This section presents our approach for multi-robot navigation with LoS connectivity maintenance. The entire framework is shown in Fig. 2. We first introduce a new metric for LoS-distance evaluation based on the polygonal visible region, and then propose a topology optimization approach to improve navigation efficiency. We focus on the 2D cases for conciseness while the formulations also apply to 3D cases. Unless specified otherwise, we assume all variables have been transformed into the local frame of an example robot $j \in \mathcal{R}$ located at \mathbf{q}_j , with $\mathbf{q}_j = [0 \ 0]^\top$.

A. Exact LoS-Distance Evaluation

To efficiently quantify the distance to the visible region, previous works directly use the determination metric d^{hull} in Eq. (3) or its variations as metrics [22], [8], [12]. However, in this paper, we define the line-of-sight distance based on the visible region \mathcal{W}_j as follows:

Definition 2 (Line-of-Sight-Distance): Given a robot i located at $\mathbf{q}_i \in \mathcal{W}_j$, the LoS-distance of a robot i to the visible

region \mathcal{W}_j of a robot j is defined as

$$d_{ji}^{\text{los}} = \min\{\|\mathbf{q}_i - \mathbf{p}\|_2 \mid \mathbf{p} \in \partial\mathcal{W}_j\},$$

where $\partial\mathcal{W}_j$ denotes the boundary of \mathcal{W}_j .

We abandon the previous metric d^{hull} or its derivatives based on our observation and analysis that, it only captures the *radial* distance to the boundary of a visible region while omitting the *tangent* distance, which leads to significant evaluation error. Moreover, the gradient of d^{hull} constrains the robot within a narrow sector with a small radial angle. Consequently, a robot with only a small lateral clearance to the boundary can neither recognize such a situation nor escape from the critical region, as illustrated in Fig. 3.

In contrast, the new metric d_{ji}^{los} evaluates the exact minimum distance from a robot i to the boundary of robot j 's visible region. However, solving the accurate d_{ji}^{los} as in Def. 2 is a non-linear optimization problem that does not have an analytical solution (details are provided in the Appendix-A). Therefore, we resort to an efficient and safe approximation of the exact d_{ji}^{los} that has a differentiable expression and supports real-time evaluation, introduced in the next subsection.

B. Visible Region Approximation

To support efficient LoS-distance evaluation, we use a 2D polygon (or polyhedron in 3D) to approximate the irregular boundaries of visible regions, as shown in Fig. 2 and Fig. 3. Specifically, given the flipped convex hull \mathcal{H}_j of a robot j , we first apply radial angle-based interpolation for each edge of \mathcal{H}_j , where the k -th edge will be interpolated with additional vertices if the radial angle θ_k spanned by this edge w.r.t. \mathbf{q}_j exceeds a predefined threshold $\Delta\theta$. After this, any two consecutive vertices on the boundary of \mathcal{H}_j will span a radial angle not exceeding $\Delta\theta$. Then, all vertices of \mathcal{H}_j , denoted as $\mathcal{V}_{\text{hull}}$, are flipped back to the original space following the flipping operation $f(\cdot)$. These vertices are sequentially connected with line segments to finally enclose an *approximated visible region* $\tilde{\mathcal{W}}_j$ to approximate \mathcal{W}_j . The detailed process is summarized in Alg. 1.

Proposition 2: The time complexity of constructing the approximated visible region $\tilde{\mathcal{W}}_j$ is $\mathcal{O}(n \log(n) + m)$, where $n = |\mathcal{C}_j|$ and $m = \frac{2\pi}{\Delta\theta}$.

The approximated visible region $\tilde{\mathcal{W}}_j$ has several advantages. First, the analytical expression of the LoS-distance to \mathcal{W}_j can be derived. Specifically, the distance of a robot i located at \mathbf{q}_i to the k -th line segment $\overline{\mathbf{a}_k \mathbf{a}_{k+1}}$ of $\tilde{\mathcal{W}}_j$ can be calculated as

$$\tilde{d}_k = \begin{cases} \|\mathbf{q}_i \mathbf{a}_k\|, & \frac{(\mathbf{q}_i \mathbf{a}_k)^\top (\mathbf{a}_{k+1} \mathbf{a}_k)}{\|\mathbf{a}_{k+1} \mathbf{a}_k\|} < 0, \\ \|\mathbf{q}_i \mathbf{a}_{k+1}\|, & \frac{(\mathbf{q}_i \mathbf{a}_k)^\top (\mathbf{a}_{k+1} \mathbf{a}_k)}{\|\mathbf{a}_{k+1} \mathbf{a}_k\|} > 1, \\ \frac{\|\mathbf{q}_i \mathbf{a}_{k+1} \times \mathbf{q}_i \mathbf{a}_k\|}{\|\mathbf{a}_k \mathbf{a}_{k+1}\|}, & \text{otherwise.} \end{cases} \quad (5)$$

The derivative of \tilde{d}_k w.r.t \mathbf{q}_i is provided in Appendix-B. We define the *approximated* LoS-distance $\tilde{d}_{ji}^{\text{los}}$ as the distance from robot i to the closest boundary of \mathcal{W}_j , calculated as

$$\tilde{d}_{ji}^{\text{los}} = \min_k \tilde{d}_k. \quad (6)$$

Since the mutual LoS-distance between two robot i and j can be different (or imbalanced) as mentioned in [12], *i.e.*, $\tilde{d}_{ji}^{\text{los}} \neq \tilde{d}_{ij}^{\text{los}}$, we take the smaller value between them as the final LoS-distance to ensure conservative evaluation, defined as $D_{ij} = \min\{\tilde{d}_{ji}^{\text{los}}, \tilde{d}_{ij}^{\text{los}}\}$. The potential function $\beta(\cdot)$ for LoS-connectivity constraints (C2) in Sec. IV-B is then defined as [12]

$$\beta_{ij} = \begin{cases} 0, & 0 \leq D_{ij} < d_{\min}^{\text{los}}, \\ \frac{k_{\beta}}{2} [1 - \cos(\frac{D_{ij} - d_{\min}^{\text{los}}}{d_{\max}^{\text{los}} - d_{\min}^{\text{los}}})\pi], & d_{\min}^{\text{los}} \leq D_{ij} < d_{\max}^{\text{los}}, \\ k_{\beta}, & D_{ij} \geq d_{\max}^{\text{los}}, \end{cases} \quad (7)$$

where $d_{\max}^{\text{los}} > 0$ is the trigger distance at which the LoS constraints take effect until robots lose LoS at $D_{ij} < d_{\min}^{\text{los}}$, with d_{\min}^{los} being a small positive margin; $k_{\beta} > 0$ is a scalar weight set to 1. It holds that $\beta_{ij} = \beta_{ji} = \beta(D_{ij})$.

The gradient direction for robot i to enhance LoS-connectivity (*i.e.*, increase β_{ij}) is given by

$$\frac{\partial \beta_{ij}}{\partial \mathbf{q}_i} = \frac{\partial \beta(\tilde{d}_{ji}^{\text{los}})}{\partial \tilde{d}_{ji}^{\text{los}}} \Big|_{\tilde{d}_{ji}^{\text{los}}=D_{ij}} \cdot \frac{\partial \tilde{d}_{ji}^{\text{los}}}{\partial \mathbf{q}_i} \quad (8)$$

However, this gradient only pushes robot i away from the boundary of \mathcal{W}_j . When robot i is free (*i.e.*, no external target) and robot j is at risk of losing LoS, we further expect robot i to *actively* move toward robot j as a relay robot for connectivity maintenance. Therefore, we reshape the gradient field by adding an additional radial component directed toward neighboring robots as follows:

$$\frac{\partial \beta_{ij}}{\partial \mathbf{q}_i} \leftarrow \frac{\partial \beta(\tilde{d}_{ji}^{\text{los}})}{\partial \tilde{d}_{ji}^{\text{los}}} \Big|_{\tilde{d}_{ji}^{\text{los}}=D_{ij}} \cdot \left(\frac{\partial \tilde{d}_{ji}^{\text{los}}}{\partial \mathbf{q}_i} + \beta(\tilde{d}_{ji}^{\text{los}}) \cdot \frac{-\mathbf{q}_i}{\|\mathbf{q}_i\|} \right). \quad (9)$$

When $\beta(\tilde{d}_{ji}^{\text{los}}) < k_{\beta}$, robot i is mainly motivated to move away from the boundary of $\tilde{\mathcal{W}}_j$ following Eq. (8); and when $\beta(\tilde{d}_{ji}^{\text{los}}) = k_{\beta}$, robot i will be further directed to chase robot j if D_{ij} is critical. Note that the gradient in Eq. (9) is defined in robot j 's local frame, and should be transformed into a global frame before being applied to robot i .

Second, we have the following propositions that guarantee $\tilde{\mathcal{W}}_j$ is a *safe* approximation of \mathcal{W}_j , in the sense that the LoS-distance will never be overestimated.

Proposition 3: The approximated visible region $\tilde{\mathcal{W}}_j$ for a robot $j \in \mathcal{R}$ is a subset of its actual visible region \mathcal{W}_j , *i.e.*, $\tilde{\mathcal{W}}_j \subseteq \mathcal{W}_j$.

Proposition 4: The approximated LoS-distance \tilde{d}^{los} is the lower bound of the exact LoS-distance d^{los} , *i.e.*, $\tilde{d}^{\text{los}} \leq d^{\text{los}}$.

The detailed proofs of Prop. 3 and Prop. 4 are provided in the Appendix C and D respectively due to space limitations.

C. Topology Optimization through Masked Graph Laplacian

In a graph Laplacian-based connectivity controller, the topology among robots is implicitly controlled by the preferred fielder eigenvalue λ_2^{\min} , *i.e.*, a larger λ_2^{\min} will result in denser connections between robots [9], [12]. However, the explicit topology specification may impose redundant connections between robots, which hinders their navigation efficiency, and sometimes leads to occasional livelocks

Algorithm 1: ApproxVisibleRegion($\mathcal{H}_j, \Delta\theta$)

```

1  $\mathcal{V}_{\text{hull}} \leftarrow []$ .
2 for  $k \in [1, 2, \dots, K]$  do
3    $\langle \mathbf{a}_k, \mathbf{a}_{k+1} \rangle \leftarrow$  the  $k$ -th edge of  $\mathcal{H}_j$ .
4   Add  $\mathbf{a}_k$  to  $\mathcal{V}_{\text{hull}}$ .
5    $\theta_k = \cos^{-1} \frac{\mathbf{a}_k^\top \mathbf{a}_{k+1}}{\|\mathbf{a}_k\| \|\mathbf{a}_{k+1}\|}$ .
6    $n_{\text{inter}} = \lfloor \theta_k / \Delta\theta \rfloor - 1$ .
7   if  $n_{\text{inter}} > 0$  then
8     Interpolate edge  $\langle \mathbf{a}_k, \mathbf{a}_{k+1} \rangle$  with  $n_{\text{inter}}$  points.
9     Sequentially add  $n_{\text{inter}}$  points to  $\mathcal{V}_{\text{hull}}$ .
10  Add  $\mathbf{a}_{k+1}$  to  $\mathcal{V}_{\text{hull}}$ .
11  $\tilde{\mathcal{W}}_j \leftarrow$  the region enclosed by connecting consecutive
    vertices in  $f(\mathcal{V}_{\text{hull}})$  with line segments.
12 return  $\tilde{\mathcal{W}}_j$ 

```

around obstacles, as shown in Fig. 6.

To address the above limitations, we propose the topology optimization above the real-time connectivity graph, where only a minimal topology $\mathcal{T}(t) \subseteq \mathcal{G}(t)$ is selected to maintain based on the following criteria: (1) $\mathcal{T}(t)$ contains no redundant edges to ensure connectivity; (2) the edges in $\mathcal{T}(t)$ require minimal efforts to maintain considering the robots' navigation movement. While quantifying these efforts is non-trivial, we circumvent explicit evaluation by directly examining the conflict between connectivity maintenance and navigational movement. Concretely, recall that the real-time edge weight in \mathcal{G} is defined as $A_{ij} = \alpha_{ij} \cdot \beta_{ij} \cdot \gamma_{ij}$, a larger A_{ij} indicates that two robots i and j are well connected under the disturbance of their navigational movements. Otherwise, A_{ij} would be small.

Therefore, we formulate the topology optimization problem as an MST search problem over $\mathcal{G}(t)$, where each edge weight is modified as

$$A_{ij}^{\text{mst}} = -\alpha_{ij} \cdot \beta_{ij} + \frac{d_{ij}}{d_{\max}^{\text{com}}}. \quad (10)$$

The first term in Eq. (10) indicates the efforts required to maintain the connectivity constraints. Note here we omit the weight γ_{ij} for collision avoidance (C3) because it is always applied between robots to ensure safety. Moreover, the second term, $\frac{d_{ij}}{d_{\max}^{\text{com}}}$, serves to prioritize shorter edges. The process of topology optimization is illustrated in Fig. 2. We use the Kruskal's algorithm to find the optimal spanning tree \mathcal{T} [23].

After obtaining the minimal topology \mathcal{T} , we mask the elements in the original generalized graph Laplacian matrix \mathbf{L} as follows:

- if $(i, j) \notin \mathcal{T}$, $A_{ij} = 0$ if $\gamma_{ij} = 1$, else $A_{ij} = \gamma_{ij}$.
- if $(i, j) \in \mathcal{T}$, A_{ij} remains unchanged;

Here $\gamma_{ij} = 1$ indicates the collision avoidance constraints (C3) are not triggered. The diagonal elements in \mathbf{L} are then modified accordingly. Note that for those edges not in \mathcal{T} , we only keep γ_{ij} to ensure safety, while eliminating their communication and LoS maintenance constraints. Based on the masked \mathbf{L} , the connectivity velocity can finally be derived

TABLE I
APPROXIMATION ERROR OF LOS-DISTANCE

r_{flip}	Metrics	$\Delta\theta$	$ \mathcal{V}^{\text{hull}} $	$t_{\text{avg}} \downarrow$	$e_{\text{avg}} \downarrow$	$e_{\text{max}} \downarrow$
150	d^{los}	—	428	1157.84	0.00	0.00
	\tilde{d}^{los}	—	428	0.16	53.25	253.94
		2	471(+10%)	0.16	1.49	4.58
		1	526(+23%)	0.17	0.34	1.20
500	d^{los}	—	577	2243.31	0.00	0.00
	\tilde{d}^{los}	—	577	0.17	19.76	119.32
		2	601(+4%)	0.17	2.82	11.65
		1	640(+11%)	0.18	0.60	1.88
1000	d^{los}	—	608	3416.79	0.00	0.00
	\tilde{d}^{los}	—	608	0.17	13.52	78.63
		2	624(+3%)	0.20	4.36	25.60
		1	655(+8%)	0.21	0.88	4.24

Notes: r_{flip} is the flipping radius (m); $\Delta\theta$, the interpolation threshold ($^\circ$); t_{avg} , the averaged computational time (ms); e_{avg} and e_{max} , the averaged and the maximum approximation errors (cm). "—" means no interpolation is performed. The percentages show the number of interpolated points w.r.t. the number of the original hull vertices.

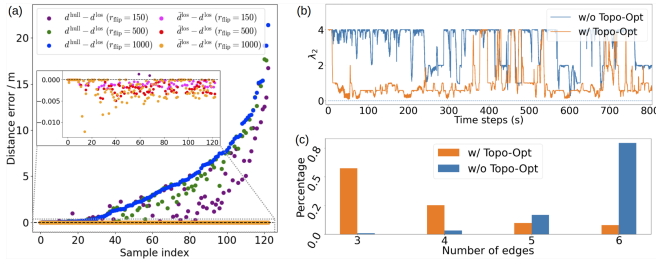


Fig. 4. (a) Error distribution of different LoS-distance metrics at uniformly sampled points in a visible region shown in Fig. 3, under various flipping radius r_{flip} . Here we set $\Delta\theta = 0.5^\circ$. (b) and (c): Ablation study of using Topo-Opt when four robots are exploring a garage environment in Fig. 1(b), where (b) compares the temporal variation of λ_2 and (c) shows the histogram of the number of connections between four robots during exploration.

following Eq. (1) as

$$\mathbf{u}_i^c = -\frac{1}{(\lambda_2 - \lambda_2^{\min})^2} \cdot \sum_{j \in \mathcal{N}_i} \frac{\partial A_{ij}}{\partial \mathbf{q}_i} \cdot (v_{2_i} - v_{2_j})^2, \quad (11)$$

where $\frac{\partial A_{ij}}{\partial \mathbf{q}_i} = \frac{\partial \alpha_{ij}}{\partial \mathbf{q}_i} \cdot \gamma_{ij} \cdot \beta_{ij} + \alpha_{ij} \cdot \frac{\partial \gamma_{ij}}{\partial \mathbf{q}_i} \cdot \beta_{ij} + \alpha_{ij} \cdot \gamma_{ij} \cdot \frac{\partial \beta_{ij}}{\partial \mathbf{q}_i}$; λ_2 and \mathbf{v}_2 are the Fiedler eigenvalue and eigenvector of \mathbf{L} .

Remark 1: The graph Laplacian-based controller may fail to maintain a specific edge in \mathcal{G} , because λ_2 is only non-decreasing (rather than strictly increasing) w.r.t. the number of edges in \mathcal{G} [19], *i.e.*, preserving a specific edge may not contribute to λ_2 . However, in our case, since we reduce \mathcal{G} to an MST by topology optimization, the λ_2 of the masked \mathbf{L} is now strictly increasing w.r.t. the number of remaining edges. Therefore, correct \mathbf{u}_i^c can be derived to maintain edges in \mathcal{T} .

Remark 2: When topology optimization is performed using distributed MST algorithms like GHS algorithm [24], the connectivity velocity in Eq. (1) can be calculated distributively by each robot, requiring only one-hop communication with its neighbors. The proof is similar to the proof in [12].

VI. EXPERIMENT RESULTS

This section evaluates the proposed framework in terms of the effectiveness of LoS-distance approximation, the robustness of connectivity maintenance, and navigation efficiency in multi-robot navigation and exploration tasks. The target assignment and the calculation of navigation velocity follow the design in [12], as shown in Fig. 2. We compare three

different metrics and several topology strategies, including a fixed topology, a graph Laplacian-based topology [12], and our proposed adaptive minimal topology, and conduct a series of ablation studies. All simulation experiments are conducted in Gazebo on a desktop with an i9-13900 CPU and 32 GB of RAM, where robots are equipped with 2D LiDARs with 360 degrees of FoV and a sensing range of 30 meters. The real-world experiments are introduced in Sec. VI-D. The laser points that hit neighboring robots are removed before constructing the visible regions. Our connectivity controller runs at 30 Hz thanks to its inherently distributed calculation.

A. Performance of LoS-Distance Approximation

This section compares the computational efficiency and approximation accuracy of the approximated LoS-distance \tilde{d}^{los} versus the exact d^{los} . The metrics are evaluated at uniformly sampled positions within the visible region in Fig. 3. As shown in Tab. I, the averaged computational time of \tilde{d}^{los} is less than one millisecond thanks to its closed-form expression, while solving d^{los} takes more than a second, which prevents it from real-time applications. Moreover, the proposed $\tilde{\mathcal{W}}_j$ well approximates the irregular boundary of the original visible region by applying radial angle-based interpolation, with average and maximum errors less than 5 cm and 30 cm, respectively, even under aggressive visible regions (*i.e.*, larger r_{flip}) and coarse interpolation.

The detailed distribution of the approximation error is shown in Fig. 4(a), where we further include the previous metric d^{hull} . Aligned with our analysis in Sec. V-A, the metric \tilde{d}^{los} is consistent with d^{los} with small approximation errors, while d^{hull} exhibits significant errors in some areas (larger than 20 meters), indicating it is unreliable as a LoS-distance metric. It is worth noting that \tilde{d}^{los} remains consistently non-positive, which experimentally validates our Prop. 4. Generally, the approximation error increases with a larger flipping radius r_{flip} and a coarser interpolation, which requires a trade-off between the accuracy and computation efficiency.

B. Robustness with Different LoS-Distance Metrics

This section evaluates the robustness of the proposed connectivity maintenance framework using different LoS-distance metrics, including d^{hull} [8], [22], $d^{\text{hull}} \cos \theta_{k^*}$ [12], and \tilde{d}^{los} (proposed). We conduct ablation studies to evaluate performance with and without topology optimization (Topo-Opt), under different trigger distance $d_{\text{max}}^{\text{los}}$ of LoS constraints, and for varying ranges of visible regions. We deploy four robots to navigate to their respective targets in an environment cluttered with small and irregular obstacles that can frequently block the LoS between robots, as shown in Fig. 1(a).

The results for LoS-connectivity maintenance are summarized in Tab. II. In general, d^{hull} and $d^{\text{hull}} \cos \theta_{k^*}$ show similar performance: they perform well when Topo-Opt is disabled and a sufficiently large trigger distance $d_{\text{max}}^{\text{los}}$ is set. However, they fail to ensure LoS connectivity under larger visible ranges when a smaller $d_{\text{max}}^{\text{los}}$ is set. Moreover, when

TABLE II
CONNECTIVITY MAINTENANCE IN MULTI-ROBOT NAVIGATION

Metrics	Topo-Opt	d_{\max}^{los} (m) ↓	r_{flip} (m) ↑		
			150	500	1000
d^{hull} [8], [22];	w/o	3.0	✓	✓	✓
	w/o	1.2	✓	×	×
$d^{\text{hull}} \cdot \cos \theta_k$ [12]	w/	3.0	×	×	×
	w/	1.2	×	×	×
\bar{d}^{los} (Proposed)	w/o	1.2	✓	✓	✓
	w/	1.2	✓	✓	✓

Notes: d_{\min}^{los} is the trigger distance for LoS constraints; d_{\min}^{los} is set to 0.1 m in all experiments. The mark ✓ indicates robots successfully navigate to their targets while maintaining connectivity, and × indicates failure.

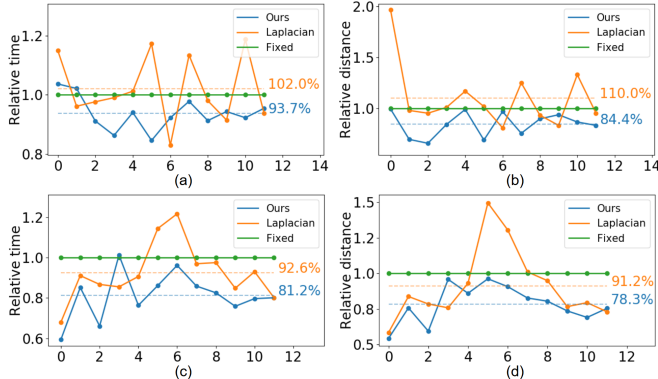


Fig. 5. Relative time and distance efficiency of compared methods with four robots navigating in a cluttered environment shown in Fig. 1(a). Dashed lines indicate the average performance. The indices of different runs are sorted in ascending order based on the total distance to the targets. (a) and (b): only one robot is assigned a random target; (c) and (d): all four robots have their targets.

redundant connections are removed with Topo-Opt, both metrics consistently fail regardless of the trigger distance and flipping radius r_{flip} . This is due to the inherent inaccuracy of d^{hull} as we previously shown in Sec. VI-A. In contrast, our metric \bar{d}^{los} can consistently preserve connectivity under both aggressive visible ranges (with $r_{\text{flip}} = 1000$ m) and fragile connectivity topology (with almost no redundant connections), verifying its reliability for LoS-distance evaluation. These advantages enable our framework to simultaneously cover a larger area while reliably maintaining minimal connections among robots.

To further showcase these advantages, we deploy the proposed framework in multi-robot exploration tasks, requiring robots to explore both structured and unstructured environments, as shown in Fig. 1(b) and (c). Despite the existence of dense obstacles, the proposed method guarantees LoS-connectivity during the exploration process, verified by the positivity of λ_2 as shown in Fig. 4(b). Moreover, our method maintains significantly fewer but necessary connections between robots when Topo-Opt is enabled, as evidenced by the histogram of the number of connections in Fig. 4(c). The results demonstrate the reliability of our framework for connectivity maintenance even under fragile topologies with fewer connections.

C. Navigation Efficiency and Applications

This section compares the navigation efficiency of related methods with different connectivity topologies, including a fixed topology (**Fixed**), the topology explicitly determined

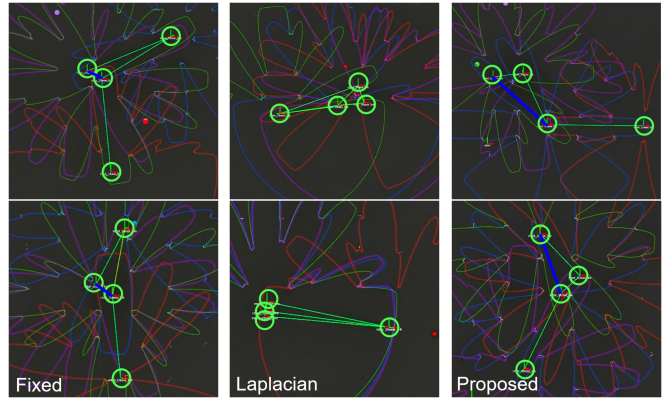


Fig. 6. Snapshots of connectivity graphs with the Fixed, Laplacian, and the proposed methods. The figure highlights the robots (green circles), selected connections (green edges), and redundant connections (blue edges). The Fixed method fails to adapt to a better topology to facilitate navigation efficiency; the Laplacian method tends to maintain redundant connections, and can lead to occasional livelock around obstacles; the proposed method adaptively optimizes the topology that facilitates navigation efficiency. The results are best appreciated with the video in supplementary materials.

by λ_2 (**Laplacian**), and the topology obtained from Topo-Opt (**Ours**). We conduct two groups of experiments with different proportions of free robots: in group (1), only one robot is assigned a target; while in group (2), all four robots have their respective targets. Each group includes twelve independent runs with randomly generated targets in the environment shown in Fig. 1(a), which contains dense and cluttered obstacles.

The relative time and distance efficiency w.r.t. the Fixed method are shown in Fig. 5. The snapshots of connectivity graphs in group (2) is also depicted in Fig. 6. In group (1) (Fig. 5(a)(b)), the Laplacian method has the worst navigation efficiency because it maintains unnecessary connections that influence the movements of unrelated robots. In group (2), (Fig. 5(c)(d)), the Fixed method shows the worst navigation efficiency as it blindly sticks to one fixed topology; the Laplacian method performs slightly better since the unnecessary connections help to alleviate conflicts in robots' navigational directions. In both settings, the proposed method shows the best time and distance efficiency on average, with around 10% and 20% improvements w.r.t. the Laplacian and the Fixed methods, respectively, thanks to the topology optimization that minimizes the interference to navigation efficiency. Moreover, the relative improvement of the distance efficiency increases from 15.6% to 21.7% as the number of free robots increases, indicating the potential of Topo-Opt in large scale multi-robot systems. Finally, it is worth noting that all methods use the proposed LoS-distance metric \bar{d}^{los} to ensure robust connectivity. This highlights the generality of our framework, which can support either the explicit minimal topology requirements (either adaptive or fixed) or the topologies implicitly determined by the Fiedler eigenvalue.

D. Real-World Experiment

We deploy the proposed method in real-world multi-robot navigation tasks with a multi-UAV system comprising three

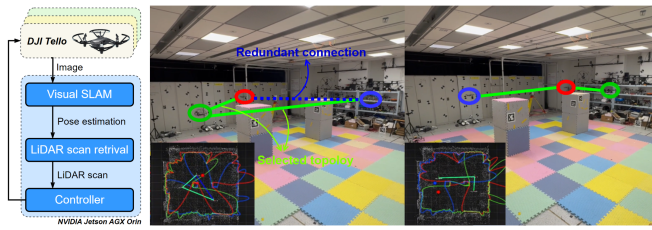


Fig. 7. Snapshots of real-world experiments where three drones navigate in an environment with obstacles. More details are in the attached videos.

DJI Tello UAVs [25], as shown in Fig. 7. Since the Tello UAV cannot mount LiDAR sensors, we pre-build a point cloud map of the environment and only use it to generate onboard LiDAR scans based on robots’ real-time visual localization with onboard cameras [26]. While we manually controlled one drone to fly around obstacles, the other two drones can autonomously move to maintain LoS-connectivity and take adaptive topologies for navigation efficiency, verifying the effectiveness of the proposed method. Notably, the entire connected multi-robot system can be deployed in unknown environments relying solely on onboard sensing and computation, underscoring its convenience and practicality for real-world deployment.

VII. CONCLUSIONS AND DISCUSSIONS

This paper proposes a LoS-connectivity maintenance method that requires no prior environment maps, based solely on robots’ real-time LiDAR scans. We propose an efficient and reliable LoS-distance metric to support LoS constraints formulation, based on the polygonal approximation of robots’ visible regions. Unnecessary and effort-demanding connections are masked out to minimize the efforts for connectivity maintenance between robots under external navigation tasks. The robustness and efficiency of the proposed method are verified with extensive multi-robot navigation experiments in challenging environments with unknown and cluttered obstacles. Future work will focus on developing learning-based methods for unified coordination between connectivity maintenance and efficient exploration, rather than treating the two modules separately.

REFERENCES

- [1] Y. Tian, K. Liu, K. Ok, L. Tran, D. Allen, N. Roy, and J. P. How, “Search and rescue under the forest canopy using multiple uavs,” *The International Journal of Robotics Research*, vol. 39, no. 10-11, pp. 1201–1221, 2020.
- [2] M. Cao, T.-M. Nguyen, S. Yuan, A. Anastasiou, A. Zacharia, S. Papaioannou, P. Kolios, C. G. Panayiotou, M. M. Polycarpou, X. Xu, et al., “Cooperative aerial robot inspection challenge: A benchmark for heterogeneous multi-uncrewed-aerial-vehicle planning and lessons learned,” *IEEE Robotics & Automation Magazine*, 2025.
- [3] R. Bai, H. Guo, W.-Y. Yau, and L. Xie, “Graph-based slam-aware exploration with prior topo-metric information,” *IEEE Robotics and Automation Letters*, vol. 9, no. 9, pp. 7597–7604, 2024.
- [4] F. Amigoni, J. Banfi, and N. Basilico, “Multirobot exploration of communication-restricted environments: A survey,” *IEEE Intelligent Systems*, vol. 32, no. 6, pp. 48–57, 2017.
- [5] G. Shi, I. E. Rabban, L. Zhou, and P. Tokekar, “Communication-aware multi-robot coordination with submodular maximization,” in *2021 IEEE International Conference on Robotics and Automation (ICRA)*, pp. 8955–8961, 2021.

- [6] J. Liu and G. Hu, “Relative localization estimation for multiple robots via the rotating ultra-wideband tag,” *IEEE Robotics and Automation Letters*, vol. 8, no. 7, pp. 4187–4194, 2023.
- [7] C. Cao, H. Zhu, Z. Ren, H. Choset, and J. Zhang, “Representation granularity enables time-efficient autonomous exploration in large, complex worlds,” *Science Robotics*, vol. 8, no. 80, p. eadf0970, 2023.
- [8] L. Xia, B. Deng, J. Pan, X. Zhang, P. Duan, B. Zhou, and H. Cheng, “RELINK: Real-time line-of-sight-based deployment framework of multi-robot for maintaining a communication network,” *IEEE Robotics and Automation Letters*, vol. 8, no. 12, pp. 8152–8159, 2023.
- [9] P. Robuffo Giordano, A. Franchi, C. Secchi, and H. H. Bühlhoff, “A passivity-based decentralized strategy for generalized connectivity maintenance,” *The International Journal of Robotics Research*, vol. 32, no. 3, pp. 299–323, 2013.
- [10] T. Nestmeyer, P. Robuffo Giordano, H. H. Bühlhoff, and A. Franchi, “Decentralized simultaneous multi-target exploration using a connected network of multiple robots,” *Autonomous robots*, vol. 41, pp. 989–1011, 2017.
- [11] Y. Chen and M. Guo, “Multi-UAV deployment in obstacle-cluttered environments with LOS connectivity,” *Arxiv 2308.12117*, 2023.
- [12] R. Bai, S. Yuan, K. Li, H. Guo, W.-Y. Yau, and L. Xie, “Realm: Real-time line-of-sight maintenance in multi-robot navigation with unknown obstacles,” in *2025 IEEE international conference on robotics and automation (ICRA)*, 2025.
- [13] Y. Yang, Y. Lyu, and W. Luo, “Minimally constrained multi-robot coordination with line-of-sight connectivity maintenance,” in *2023 IEEE international conference on robotics and automation (ICRA)*, pp. 7684–7690, 2023.
- [14] E. Stump, N. Michael, V. Kumar, and V. Isler, “Visibility-based deployment of robot formations for communication maintenance,” in *2011 IEEE international conference on robotics and automation (ICRA)*, pp. 4498–4505, 2011.
- [15] G. A. Hollinger and S. Singh, “Multirobot coordination with periodic connectivity: Theory and experiments,” *IEEE Transactions on Robotics*, vol. 28, no. 4, pp. 967–973, 2012.
- [16] A. Dutta, A. Ghosh, and O. P. Kreidl, “Multi-robot informative path planning with continuous connectivity constraints,” in *2019 International Conference on Robotics and Automation (ICRA)*, pp. 3245–3251, May 2019.
- [17] W. Luo, S. Yi, and K. Sycara, “Behavior mixing with minimum global and subgroup connectivity maintenance for large-scale multi-robot systems,” in *2020 IEEE international conference on robotics and automation (ICRA)*, pp. 9845–9851, 2020.
- [18] F. Yang, C. Cao, H. Zhu, J. Oh, and J. Zhang, “FAR Planner: Fast, attemptable route planner using dynamic visibility update,” in *2022 IEEE/RSJ International Conference on Intelligent Robots and Systems (IROS)*, pp. 9–16, 2022.
- [19] M. Fiedler, “Algebraic connectivity of graphs,” *Czechoslovak mathematical journal*, vol. 23, no. 2, pp. 298–305, 1973.
- [20] P. Yang, R. A. Freeman, G. J. Gordon, K. M. Lynch, S. S. Srinivasa, and R. Sukthankar, “Decentralized estimation and control of graph connectivity for mobile sensor networks,” *Automatica*, vol. 46, no. 2, pp. 390–396, 2010.
- [21] S. Katz, A. Tal, and R. Basri, “Direct visibility of point sets,” in *ACM SIGGRAPH 2007 papers*, pp. 24–es, 2007.
- [22] T. Liu, Q. Wang, X. Zhong, Z. Wang, C. Xu, F. Zhang, and F. Gao, “Star-convex constrained optimization for visibility planning with application to aerial inspection,” in *2022 IEEE International Conference on Robotics and Automation (ICRA)*, pp. 7861–7867, 2022.
- [23] J. B. Kruskal, “On the shortest spanning subtree of a graph and the traveling salesman problem,” *Proceedings of the American Mathematical society*, vol. 7, no. 1, pp. 48–50, 1956.
- [24] R. G. Gallager, P. A. Humblet, and P. M. Spira, “A distributed algorithm for minimum-weight spanning trees,” *ACM Transactions on Programming Languages and systems (TOPLAS)*, vol. 5, no. 1, pp. 66–77, 1983.
- [25] X. Li, K. Xu, F. Liu, R. Bai, S. Yuan, and L. Xie, “Airswarm: Enabling cost-effective multi-uav research with cots drones,” in *2025 IEEE/RSJ International Conference on Intelligent Robots and Systems (IROS)*, 2025.
- [26] K. Xu, Y. Hao, S. Yuan, C. Wang, and L. Xie, “Airsam: An efficient and illumination-robust point-line visual slam system,” *IEEE Transactions on Robotics*, 2025.

A. Formulation of Solving Exact LoS-Distance

To obtain the accurate LoS-distance d_{ji}^{los} as in Def. 2, we have to solve the following nonlinear optimization problem:

$$\min_{\mathbf{p}} \|\mathbf{p} - \mathbf{q}_i\|_2, \quad (12)$$

$$\text{s.t. } i) \mathbf{p} = f(\mathbf{p}'); \quad ii) \sum_k z_k = 1, z_k \in \{0, 1\};$$

$$iii) \mathbf{p}' = \sum_k z_k (\alpha \mathbf{a}_k + (1 - \alpha) \mathbf{a}_{k+1}), \alpha \in [0, 1].$$

The above constraints (i-iii) restrict that the point \mathbf{p} is located at the boundary of \mathcal{W}_j , with a corresponding convex hull \mathcal{H}_j with K edges. Finding the optimal \mathbf{p}^* involves solving a high-order equation that generally does not have an analytical solution. In this work, we solve the above non-linear program using Gurobi. The time efficiency of solving the problem in 2D case is compared in Tab. I.

B. Gradient of Approximated LoS-Distance

Following the definition of \tilde{d}_k in Eq. (5), the gradient of \tilde{d}_k is derived as

$$\frac{\partial \tilde{d}_k}{\partial \mathbf{q}_i} = \begin{cases} \frac{\mathbf{q}_i \mathbf{a}_k}{\|\mathbf{q}_i \mathbf{a}_k\|}, & \frac{(\mathbf{q}_i \mathbf{a}_k)^\top (\mathbf{a}_{k+1} \mathbf{a}_k)}{\|\mathbf{a}_{k+1} \mathbf{a}_k\|} < 0, \\ \frac{\mathbf{q}_i \mathbf{a}_{k+1}}{\|\mathbf{q}_i \mathbf{a}_{k+1}\|}, & \frac{(\mathbf{q}_i \mathbf{a}_k)^\top (\mathbf{a}_{k+1} \mathbf{a}_k)}{\|\mathbf{a}_{k+1} \mathbf{a}_k\|} > 1, \\ \frac{(\mathbf{q}_i \mathbf{a}_k)}{d_k} - \frac{(\mathbf{a}_{k+1} \mathbf{a}_k)^\top (\mathbf{q}_i \mathbf{a}_k) (\mathbf{a}_{k+1} \mathbf{a}_k)}{d_k \|\mathbf{a}_{k+1} \mathbf{a}_k\|^2}, & \text{otherwise.} \end{cases} \quad (13)$$

The gradient of the approximated LoS-distance can push a robot away from the closest boundary of the neighboring robot's visible region, thereby maintaining LoS-connectivity.

C. Proof of Proposition 3

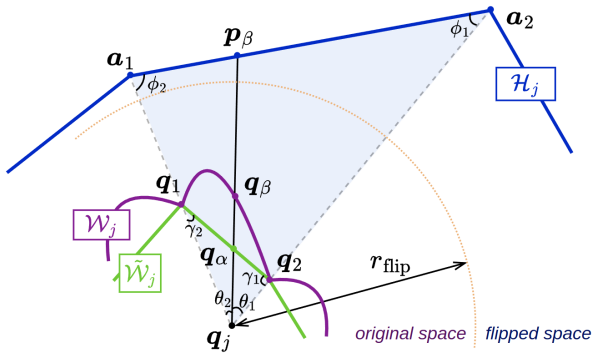


Fig. 8. Illustration of notations used in the proof of Prop. 3.

Proof: As shown in Fig. 8, the boundary of \mathcal{W}_j is described by several segments of curves, each of which (e.g., $\widehat{\mathbf{q}_1 \mathbf{q}_2}$) is obtained by flipping one edge (e.g., $\langle \mathbf{a}_1, \mathbf{a}_2 \rangle$) of the convex hull \mathcal{H}_j from the flipped space back to the original space. To prove $\tilde{\mathcal{W}}_j \subseteq \mathcal{W}_j$, it is equivalent to prove that $\forall k \in [1, 2, \dots, K]$, $(\tilde{\mathcal{W}}_j \cap \Delta \mathbf{q}_j \mathbf{a}_k \mathbf{a}_{k+1}) \subseteq (\mathcal{W}_j \cap \Delta \mathbf{q}_j \mathbf{a}_k \mathbf{a}_{k+1})$, where $\Delta \mathbf{q}_j \mathbf{a}_k \mathbf{a}_{k+1}$ denotes the triangle formed by three points $(\mathbf{q}_j, \mathbf{a}_k, \mathbf{a}_{k+1})$, and $\langle \mathbf{a}_k, \mathbf{a}_{k+1} \rangle$ is the k -th edge of \mathcal{H}_j .

We take the edge $\langle \mathbf{a}_1, \mathbf{a}_2 \rangle$ of \mathcal{H}_j as an example, as shown in Fig. 8. The corresponding boundaries of \mathcal{W}_j and $\tilde{\mathcal{W}}_j$ are denoted as a curve $\widehat{\mathbf{q}_1 \mathbf{q}_2}$ and a line segment $\overline{\mathbf{q}_1 \mathbf{q}_2}$ respectively. By construction, it holds that $\mathbf{a}_1 = f(\mathbf{q}_1)$ and $\mathbf{a}_2 = f(\mathbf{q}_2)$, where $f(\cdot)$ denotes the flipping operation. We take a random point $\mathbf{q}_\alpha = \mathbf{q}_2 + \alpha(\mathbf{q}_1 - \mathbf{q}_2)$ with $\alpha \in [0, 1]$ on $\overline{\mathbf{q}_1 \mathbf{q}_2}$. The ray from \mathbf{q}_j to \mathbf{q}_α will intersect with $\widehat{\mathbf{q}_1 \mathbf{q}_2}$ at \mathbf{q}_β , and will also intersect with $\overline{\mathbf{a}_1 \mathbf{a}_2}$ at \mathbf{a}_β , where \mathbf{a}_β can be defined as $\mathbf{a}_\beta = \mathbf{a}_2 + \beta(\mathbf{a}_1 - \mathbf{a}_2)$ with $\beta \in [0, 1]$. Note that β can be different from α .

By definition, both \mathcal{W}_j and $\tilde{\mathcal{W}}_j$ are stat-convex polytopes with \mathbf{q}_j being the center, i.e., for any point $\mathbf{q} \in \mathcal{W}_j$, the line segment $\overline{\mathbf{q}_j \mathbf{q}}$ lies entirely within \mathcal{W}_j . The same property also holds for $\tilde{\mathcal{W}}_j$. Therefore, to prove $\tilde{\mathcal{W}}_j \subseteq \mathcal{W}_j$, it is sufficient to prove that for any point \mathbf{q}_α on the boundary $\widehat{\mathbf{q}_1 \mathbf{q}_2}$, and the corresponding point \mathbf{q}_β on the boundary $\overline{\mathbf{q}_1 \mathbf{q}_2}$, it holds that $\|\mathbf{q}_j \mathbf{q}_\alpha\| \leq \|\mathbf{q}_j \mathbf{q}_\beta\|$. Otherwise, if $\|\mathbf{q}_j \mathbf{q}_\alpha\| > \|\mathbf{q}_j \mathbf{q}_\beta\|$, the line segment $\overline{\mathbf{q}_\alpha \mathbf{q}_\beta} \subseteq \tilde{\mathcal{W}}_j$ and $\overline{\mathbf{q}_\alpha \mathbf{q}_\beta} \not\subseteq \mathcal{W}_j$, which contradicts with $\tilde{\mathcal{W}}_j \subseteq \mathcal{W}_j$. In the following, we will prove that $\|\mathbf{q}_j \mathbf{q}_\alpha\| \leq \|\mathbf{q}_j \mathbf{q}_\beta\|$, $\forall \alpha \in [0, 1]$.

First, by applying the Law of Sines in $\Delta \mathbf{q}_j \mathbf{q}_\alpha \mathbf{q}_2$, it holds that

$$\frac{\alpha \cdot \|\mathbf{q}_1 \mathbf{q}_2\|}{\sin \theta_1} = \frac{\|\mathbf{q}_j \mathbf{q}_\alpha\|}{\sin \gamma_1}, \quad (14)$$

and

$$\frac{(1 - \alpha) \cdot \|\mathbf{q}_1 \mathbf{q}_2\|}{\sin \theta_2} = \frac{\|\mathbf{q}_j \mathbf{q}_\alpha\|}{\sin \gamma_2}. \quad (15)$$

Also in $\Delta \mathbf{q}_j \mathbf{q}_1 \mathbf{q}_2$, it holds that

$$\frac{\|\mathbf{q}_j \mathbf{q}_1\|}{\sin \gamma_1} = \frac{\|\mathbf{q}_j \mathbf{q}_2\|}{\sin \gamma_2} = \frac{\|\mathbf{q}_1 \mathbf{q}_2\|}{\sin \theta}, \quad (16)$$

where $\theta = \theta_1 + \theta_2$. By eliminating $\sin \gamma_1$ and $\sin \gamma_2$ in Eq. (14) and (15), α can be expressed as

$$\alpha = \frac{\sin \theta_1 \cdot \|\mathbf{q}_j \mathbf{q}_2\|}{\sin \theta_2 \cdot \|\mathbf{q}_j \mathbf{q}_1\| + \sin \theta_1 \cdot \|\mathbf{q}_j \mathbf{q}_2\|}. \quad (17)$$

Similarly,

$$\beta = \frac{\sin \theta_1 \cdot \|\mathbf{q}_j \mathbf{a}_2\|}{\sin \theta_2 \cdot \|\mathbf{q}_j \mathbf{a}_1\| + \sin \theta_1 \cdot \|\mathbf{q}_j \mathbf{a}_2\|}. \quad (18)$$

Combining Eq. (14) and Eq. (16), it holds that

$$\|\mathbf{q}_j \mathbf{q}_\alpha\| = \frac{\alpha \cdot \|\mathbf{q}_j \mathbf{q}_1\| \cdot \sin \theta}{\sin \theta_1}. \quad (19)$$

Similarly,

$$\|\mathbf{q}_j \mathbf{a}_\beta\| = \frac{\beta \cdot \|\mathbf{q}_j \mathbf{a}_1\| \cdot \sin \theta}{\sin \theta_1}. \quad (20)$$

To prove $\|\mathbf{q}_j \mathbf{q}_\alpha\| \leq \|\mathbf{q}_j \mathbf{a}_\beta\|$, it is equivalent to prove that

$$\begin{aligned} & 2r_{\text{flip}} - \|\mathbf{q}_j \mathbf{q}_\alpha\| \geq \|\mathbf{q}_j \mathbf{a}_\beta\| \\ \Rightarrow & 2r_{\text{flip}} \sin \theta_1 - \alpha \cdot \|\mathbf{q}_j \mathbf{q}_1\| \cdot \sin \theta \geq \beta \cdot \|\mathbf{q}_j \mathbf{a}_1\| \sin \theta \\ \Rightarrow & 2r_{\text{flip}} \geq \frac{\sin \theta}{\sin \theta_1} \cdot \alpha \cdot \|\mathbf{q}_j \mathbf{q}_1\| + \frac{\sin \theta}{\sin \theta_1} \cdot \beta \cdot \|\mathbf{q}_j \mathbf{a}_1\| = \text{RHS} \end{aligned} \quad (21)$$

Taking Eq. (17) and (18) into Eq. (21), the right-hand-side

(RHS) of Eq. (21) can be expanded as

$$\begin{aligned}
RHS &= \frac{\sin \theta \cdot \|\mathbf{q}_j \mathbf{q}_1\| \cdot \|\mathbf{q}_j \mathbf{q}_2\|}{\sin \theta_2 \cdot \|\mathbf{q}_j \mathbf{q}_1\| + \sin \theta_1 \cdot \|\mathbf{q}_j \mathbf{q}_2\|} + \\
&\quad \frac{\sin \theta \cdot \|\mathbf{q}_j \mathbf{a}_1\| \cdot \|\mathbf{q}_j \mathbf{a}_2\|}{\sin \theta_2 \cdot \|\mathbf{q}_j \mathbf{a}_1\| + \sin \theta_1 \cdot \|\mathbf{q}_j \mathbf{a}_2\|} \\
&= \frac{\|\mathbf{q}_j \mathbf{q}_1\| \cdot \|\mathbf{q}_j \mathbf{q}_2\|}{\frac{\sin \theta_2}{\sin \theta} \cdot \|\mathbf{q}_j \mathbf{q}_1\| + \frac{\sin \theta_1}{\sin \theta} \cdot \|\mathbf{q}_j \mathbf{q}_2\|} + \\
&\quad \frac{\|\mathbf{q}_j \mathbf{a}_1\| \cdot \|\mathbf{q}_j \mathbf{a}_2\|}{\frac{\sin \theta_2}{\sin \theta} \cdot \|\mathbf{q}_j \mathbf{a}_1\| + \frac{\sin \theta_1}{\sin \theta} \cdot \|\mathbf{q}_j \mathbf{a}_2\|}
\end{aligned} \tag{22}$$

The function $h_\theta(x) = \frac{\sin x}{\sin \theta} \geq \frac{x}{\theta}$ when $x \in [0, \theta]$, and $\frac{\sin x}{\sin \theta} = \frac{x}{\theta}$ only when $x = 0$ or $x = \theta$. Therefore, the RHS of Eq. (22) satisfies

$$RHS \leq \frac{\|\mathbf{q}_j \mathbf{q}_1\| \cdot \|\mathbf{q}_j \mathbf{q}_2\|}{\frac{\theta_2}{\theta} \|\mathbf{q}_j \mathbf{q}_1\| + \frac{\theta_1}{\theta} \|\mathbf{q}_j \mathbf{q}_2\|} + \frac{\|\mathbf{q}_j \mathbf{a}_1\| \cdot \|\mathbf{q}_j \mathbf{a}_2\|}{\frac{\theta_2}{\theta} \|\mathbf{q}_j \mathbf{a}_1\| + \frac{\theta_1}{\theta} \|\mathbf{q}_j \mathbf{a}_2\|}. \tag{23}$$

As $\theta_1, \theta_2, \theta > 0$, and $\theta_1 + \theta_2 = \theta$, we define $\eta = \frac{\theta_2}{\theta} \in [0, 1]$ to replace θ_1, θ_2 and θ . The Eq. (23) can be written as

$$RHS \leq \frac{\|\mathbf{q}_j \mathbf{q}_1\| \cdot \|\mathbf{q}_j \mathbf{q}_2\|}{\eta \|\mathbf{q}_j \mathbf{q}_1\| + (1-\eta) \|\mathbf{q}_j \mathbf{q}_2\|} + \frac{\|\mathbf{q}_j \mathbf{a}_1\| \cdot \|\mathbf{q}_j \mathbf{a}_2\|}{\eta \|\mathbf{q}_j \mathbf{a}_1\| + (1-\eta) \|\mathbf{q}_j \mathbf{a}_2\|}. \tag{24}$$

Note that $\|\mathbf{q}_j \mathbf{a}_1\| = 2r_{\text{flip}} - \|\mathbf{q}_j \mathbf{q}_1\|$, $\|\mathbf{q}_j \mathbf{a}_2\| = 2r_{\text{flip}} - \|\mathbf{q}_j \mathbf{q}_2\|$, we have $\eta \cdot \|\mathbf{q}_j \mathbf{a}_1\| + (1-\eta) \cdot \|\mathbf{q}_j \mathbf{a}_2\| = 2r_{\text{flip}} - (\eta \cdot \|\mathbf{q}_j \mathbf{q}_1\| + (1-\eta) \cdot \|\mathbf{q}_j \mathbf{q}_2\|)$. Let x be an auxiliary variable defined as $x = \eta \cdot \|\mathbf{q}_j \mathbf{q}_1\| + (1-\eta) \cdot \|\mathbf{q}_j \mathbf{q}_2\|$, which takes values from $\min\{\|\mathbf{q}_j \mathbf{q}_1\|, \|\mathbf{q}_j \mathbf{q}_2\|\}$ to $\max\{\|\mathbf{q}_j \mathbf{q}_1\|, \|\mathbf{q}_j \mathbf{q}_2\|\}$. The Eq. (24) can be rewritten as

$$RHS \leq \frac{\|\mathbf{q}_j \mathbf{q}_1\| \cdot \|\mathbf{q}_j \mathbf{q}_2\|}{x} + \frac{\|\mathbf{q}_j \mathbf{a}_1\| \cdot \|\mathbf{q}_j \mathbf{a}_2\|}{2r_{\text{flip}} - x} = g(x). \tag{25}$$

The derivative of $g(x)$ is calculated as

$$\begin{aligned}
\frac{\partial g(x)}{\partial x} &= \frac{-\|\mathbf{q}_j \mathbf{q}_1\| \cdot \|\mathbf{q}_j \mathbf{q}_2\|}{x^2} + \frac{-\|\mathbf{q}_j \mathbf{a}_1\| \cdot \|\mathbf{q}_j \mathbf{a}_2\|}{(2r_{\text{flip}} - x)^2} \\
&= \frac{Ax^2 + Bx - C}{x^2(2r_{\text{flip}} - x)^2},
\end{aligned} \tag{26}$$

where $A = \|\mathbf{q}_j \mathbf{a}_1\| \cdot \|\mathbf{q}_j \mathbf{a}_2\| - \|\mathbf{q}_j \mathbf{q}_1\| \cdot \|\mathbf{q}_j \mathbf{q}_2\|$, $B = 4r_{\text{flip}} \cdot \|\mathbf{q}_j \mathbf{q}_1\| \cdot \|\mathbf{q}_j \mathbf{q}_2\|$, $C = 4r_{\text{flip}}^2 \cdot \|\mathbf{q}_j \mathbf{q}_1\| \cdot \|\mathbf{q}_j \mathbf{q}_2\|$. The sign of $\frac{\partial g(x)}{\partial x}$ depends on the quadratic function $Ax^2 + Bx - C$. Since $\|\mathbf{q}_j \mathbf{a}_1\| > r_{\text{flip}}$, $\|\mathbf{q}_j \mathbf{q}_1\| < r_{\text{flip}}$, we have $\|\mathbf{q}_j \mathbf{a}_1\| > \|\mathbf{q}_j \mathbf{q}_1\|$. Similarly, it holds that $\|\mathbf{q}_j \mathbf{a}_2\| > \|\mathbf{q}_j \mathbf{q}_2\|$. Therefore, $A > 0$; the axis of symmetry is $-\frac{B}{2A} < 0$; and the function has two roots because the discriminant $B^2 + 4AC > 0$. Therefore, according to the properties of a univariate quadratic curve, the function $g(x)$ has two possible trends within the domain of x : (1) $g(x)$ decreases first and then increases; (2) $g(x)$ increases monotonically. In both cases, the maximum value of $g(x)$ is achieved on the boundary of the domain of x . When $x = \|\mathbf{q}_j \mathbf{q}_1\|$, $g(x) = 2r_{\text{flip}}$; and when $x = \|\mathbf{q}_j \mathbf{q}_2\|$, $g(x) = 2r_{\text{flip}}$. Therefore, it holds that

$$RHS \leq g(x) \leq 2r_{\text{flip}}, \tag{27}$$

which proves Eq. 21. Consequently, $\|\mathbf{q}_j \mathbf{q}_\alpha\| \leq \|\mathbf{q}_j \mathbf{q}_\beta\|$, $\forall \alpha \in [0, 1]$. And for a convex hull \mathcal{H}_j with K edges, it holds that $(\mathcal{W}_j \cap \Delta_{\mathbf{q}_j \mathbf{a}_k \mathbf{a}_{k+1}}) \subseteq (\mathcal{W}_j \cap \Delta_{\mathbf{q}_j \mathbf{a}_k \mathbf{a}_{k+1}})$, $\forall k \in [1, \dots, K]$. This concludes the proof of $\mathcal{W}_j \subseteq \mathcal{W}_j$. ■

With Prop. 3, we have the following corollary:

Corollary 1: $\forall k \in [1, \dots, K]$, the region $\mathcal{W}_j \cap \Delta_{\mathbf{q}_j \mathbf{a}_k \mathbf{a}_{k+1}}$ is convex, where $\Delta_{\mathbf{q}_j \mathbf{a}_k \mathbf{a}_{k+1}}$ denotes the triangle formed by three points $\langle \mathbf{q}_j, \mathbf{a}_k, \mathbf{a}_{k+1} \rangle$.

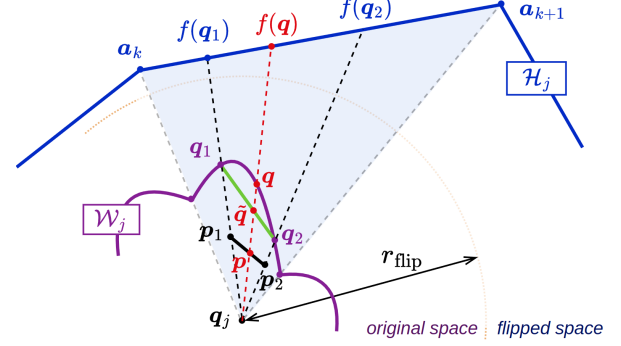


Fig. 9. Illustration of notations used in the proof of Cor. 1.

Proof: Let $\mathbf{p}_1, \mathbf{p}_2$ be two random points within $\mathcal{W}_j \cap \Delta_{\mathbf{q}_j \mathbf{a}_k \mathbf{a}_{k+1}}$, as shown in Fig. 9. If $\forall \alpha \in [0, 1]$, $\alpha \mathbf{p}_1 + (1-\alpha) \mathbf{p}_2 \in \mathcal{W}_j \cap \Delta_{\mathbf{q}_j \mathbf{a}_k \mathbf{a}_{k+1}}$, then the region $\mathcal{W}_j \cap \Delta_{\mathbf{q}_j \mathbf{a}_k \mathbf{a}_{k+1}}$ is convex.

By construction, the region $\mathcal{W}_j \cap \Delta_{\mathbf{q}_j \mathbf{a}_k \mathbf{a}_{k+1}}$ is star-convex. Therefore, the ray originating from \mathbf{p}_j to $\mathbf{p}_1, \mathbf{p}_2$ will intersect with the boundary of \mathcal{W}_j at \mathbf{q}_1 and \mathbf{q}_2 , respectively; and it holds that $\|\mathbf{p}_1\| \leq \|\mathbf{q}_1\|$ and $\|\mathbf{p}_2\| \leq \|\mathbf{q}_2\|$. Let $\mathbf{p} = \alpha \mathbf{p}_1 + (1-\alpha) \mathbf{p}_2$ be a randomly selected point on the line segment $\overline{\mathbf{p}_1 \mathbf{p}_2}$, and the ray from \mathbf{q}_j to \mathbf{p} intersect with $\overline{\mathbf{q}_1 \mathbf{q}_2}$, \mathcal{W}_j and $\overline{\mathbf{a}_k \mathbf{a}_{k+1}}$ at $\tilde{\mathbf{q}}, \mathbf{q}$ and $f(\mathbf{q})$ respectively, as shown in Fig. 9. If $\|f(\mathbf{p})\| > \|f(\mathbf{q})\|$, it holds that $\mathbf{p} \in \mathcal{W}_j \cap \Delta_{\mathbf{q}_j \mathbf{a}_k \mathbf{a}_{k+1}}$ according to visibility determination as in Prop. 1, which then proves Cor. 1.

Recall that $f(\cdot)$ is the spherical flipping function. It holds that

$$\|f(\mathbf{p})\| = 2r_{\text{flip}} - \|\mathbf{p}\| \geq 2r_{\text{flip}} - \|\tilde{\mathbf{q}}\| = \|f(\tilde{\mathbf{q}})\|. \tag{28}$$

Note that the second inequality holds because $\mathbf{p} \in \Delta_{\mathbf{q}_j \mathbf{q}_1 \mathbf{q}_2}$, and $\Delta_{\mathbf{q}_j \mathbf{q}_1 \mathbf{q}_2}$ is also star-convex. We have proved similarly in the proof of Prop. 3 that $\|f(\tilde{\mathbf{q}})\| \geq \|f(\mathbf{q})\|$. Therefore, $\|f(\mathbf{p})\| \geq \|f(\mathbf{q})\|$; and $\mathbf{p} \in \mathcal{W}_j \cap \Delta_{\mathbf{q}_j \mathbf{a}_k \mathbf{a}_{k+1}}$, $\forall \alpha \in [0, 1]$. This proves that the region $\mathcal{W}_j \cap \Delta_{\mathbf{q}_j \mathbf{a}_k \mathbf{a}_{k+1}}$ is convex. ■

D. Proof of Proposition 4

Proof: We prove Prop. 4 by contradiction. Assume that the approximated LoS-distance $\tilde{d}_{ji}^{\text{los}} > d_{ji}^{\text{los}}$, the circle $\tilde{\mathcal{S}}$ (or sphere in 3D) centered at robot i with radius $\tilde{d}_{ji}^{\text{los}}$ will cover a larger area than the circle \mathcal{S} with radius d_{ji}^{los} , i.e., $\mathcal{S} \subset \tilde{\mathcal{S}} \subseteq \tilde{\mathcal{W}}_j$. According to Prop. 3, $\tilde{\mathcal{W}}_j \subseteq \mathcal{W}_j$, it holds that $\tilde{\mathcal{S}} \subseteq \tilde{\mathcal{W}}_j \subseteq \mathcal{W}_j$. Therefore, the distance from \mathbf{q}_j to the boundary of \mathcal{W}_j is not smaller than $\tilde{d}_{ji}^{\text{los}}$, i.e., $d_{ji}^{\text{los}} \geq \tilde{d}_{ji}^{\text{los}}$, which contradicts with $\tilde{d}_{ji}^{\text{los}} > d_{ji}^{\text{los}}$. This proves Prop. 4. ■